Studies on Spin-equilibrium Iron(III) Complexes. Part 1. Syntheses and Magnetic Properties of a New Family of Spin Cross-over Iron(III) Complexes with a Unidentate Ligand over a Wide Range of the Spectrochemical Series and a Quinquedentate Ligand derived from Salicylaldehyde and Di(3-aminopropyl)amine. *X*-Ray Crystal Structure of [4-Azaheptamethylene-1,7-bis(salicylideneiminato)](4-methylpyridine)iron(III) Tetraphenylborate†

Naohide Matsumoto,* Shoichi Ohta, Chikako Yoshimura, and Akira Ohyoshi
Department of Synthetic Chemistry, Faculty of Engineering, Kumamoto University, Kurokami 2-39-1, Kumamoto 860, Japan
Susumu Kohata
Yatsushiro College of Technology, Hirayama-shinmachi, Yatsushiro 866, Japan
Hisashi Okawa and Yonezo Maeda
Department of Chemistry, Faculty of Science, Kyushu University, Hakozaki, Higashi-ku, Fukuoka 812, Japan

Iron(III) complexes of general formula $[Fe(X)L]^{n+}$ ($n = 0$ or 1) have been prepared and characterized, where X is a unidentate ligand such as Cl^-, N_3^-, NCO^-, CN^-, pyridine (py), 3-methylpyridine (3Me-py), 4-methylpyridine (4Me-py), 4-aminopyridine (apy), 3,4-dimethylpyridine ($3,4Me_2$-py), imidazole (Him), *N*-methylimidazole (mim), or 2-methylimidazole (2Me-im), and L denotes a quinquedentate Schiff base derived from salicylaldehyde and di(3-aminopropyl)amine. On the basis of the cryomagnetic data, these complexes can be classified into three groups: high spin ($S = \frac{5}{2}$) for X = Cl, N_3, Him, mim; low spin ($S = \frac{1}{2}$) for X = CN; spin cross-over ($S = \frac{1}{2} \rightleftarrows S = \frac{5}{2}$) for X = py, 3Me-py, 4Me-py, $3,4Me_2$-py, 2Me-im. This indicates that the spin state for the series of complexes depends predominantly on the order in the spectrochemical series of the ligand X. The magnetic moments for the spin cross-over complexes increased gradually with increase of the temperature and showed no thermal hysteresis, indicating that the present complexes are of continuous spin-transition type. The spin cross-over complexes showed a thermochromism both in the solids and solutions, changing colour from dark violet to blue green, with decreasing temperature, and the thermochromism was studied by the temperature dependence of the electronic spectra in dichloromethane solution. The temperature dependence of the Mössbauer spectra for $[Fe(2Me\text{-}im)L]BPh_4$ and $[Fe(4Me\text{-}py)L]BPh_4$ has also provided evidence that the spin transition between the high- and low-spin states takes place and that the rate of spin interexchange is as fast as the inverse of the lifetime (1×10^{-7} s) of the Mössbauer nucleus. One of the complexes, $[Fe(4Me\text{-}py)L]BPh_4$, was also subjected to a single-crystal *X*-ray analysis. The result verified the detailed structure in which the iron(III) atom assumes a pseudo-octahedral co-ordination geometry with a *trans* geometry for the two salicylideneiminate moieties, and the two axial positions are occupied by the secondary amine nitrogen of the di(3-aminopropyl)amine moiety of L and the nitrogen atom of the 4-methylpyridine ligand.

Tanabe and Sugano[1] calculated the energy levels of d^n electronic configurations in the octahedral ligand field. According to their diagram for the d^5 configuration, the ground state changes from ^6A to ^2T at cross-over point, when the ligand field strength (Dq/B) is increased, and it is expected that there are three types of iron(III) complexes in the octahedral field depending on the ligand field strength, that is high-spin ($S = \frac{5}{2}$), low-spin ($S = \frac{1}{2}$), and spin cross-over ($S = \frac{5}{2} \rightleftarrows S = \frac{1}{2}$) complexes. In fact, three types of complexes are known for a number of tris(dialkyldithiocarbamato)iron(III) complexes and iron(III) complexes with sexidentate Schiff bases derived from various salicylaldehydes (or acetylacetone) and linear tetramine.[2-7] In such complexes, the chelate ring size, substituent, counter ion, and solvation affect the spin state of iron(III) in a complex way and it is not appropriate to examine the theory of Tanabe and Sugano[1] systematically.

In this study, a series of six-co-ordinated iron(III) complexes with a quinquedentate ligand (L) and a variety of single unidentate ligands (X) (Figure 1) has been prepared, in order to investigate the Tanabe–Sugano theory experimentally. In the series of the present iron(III) complexes of general formula $[Fe(X)L]^{n+}$ ($n = 0$ or 1), L was kept constant and only the unidentate ligand X was varied over a wide range of the spectrochemical series (*i.e.*, ligand field strength of X), so that this series of iron(III) complexes is a good experimental system to confirm the Tanabe–Sugano theory.

The complexes were characterized by elemental analyses, melting points, i.r. spectra, electrical conductivities, temperature dependences of the electronic spectra, Mössbauer spectra, magnetic susceptibilities, and differential scanning calorimetry (d.s.c.). One of the complexes, $[Fe(4Me\text{-}py)L]BPh_4$, has been subjected to single-crystal *X*-ray analysis, in order to confirm the detailed structure.

† *Supplementary data available* (No. SUP 56320, 4 pp.): H-atom co-ordinates, anisotropic thermal parameters. See Instructions for Authors, *J. Chem. Soc., Dalton Trans.*, 1985, Issue 1, pp. xvii—xix. Structure factors are available from the editorial office.

Non-S.I. units employed: cal = 4.184 J, B.M. = 9.274×10^{-24} J T^{-1}, c.g.s.u. = $\frac{10^7}{4\pi}$ S.I. unit.

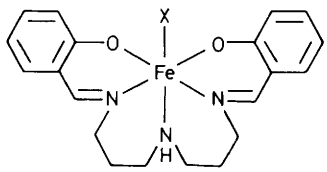

Figure 1. Schematic structure for $[Fe(X)L]^{n+}$ (n = 0 or 1), where L = 4-azaheptamethylene-1,7-bis(salicylideneiminate) and X = Cl, N_3, NCO, CN, pyridine (py), 3-methylpyridine (3Me-py), 4-methylpyridine (4Me-py), 4-aminopyridine(apy), 3,4-dimethylpyridine (3,4Me_2-py), imidazole (Him), *N*-methylimidazole (mim), or 2-methylimidazole (2Me-im)

Experimental

Syntheses.—*Neutral ligand* H_2L. The quinquedentate ligand was prepared by mixing salicylaldehyde (0.2 mol) and di(3-aminopropyl)amine (0.1 mol) in methanol (100 cm^3). The ligand is obtained as a yellow oily material and was used subsequently for the preparation of the chloro-iron(III) complex [Fe(Cl)L].

Complex [Fe(Cl)L]. To a solution of H_2L (10 mmol) in methanol (50 cm^3) was added a solution of anhydrous iron(III) chloride (10 mmol) in methanol (50 cm^3). The mixture was stirred at 50 °C for 10 min and then triethylamine (20 mmol) was added. The resulting solution was stirred at 50 °C for 1 h, during which time black crystals precipitated. They were collected, washed with methanol and diethyl ether, and dried *in vacuo*.

Complexes [Fe(X)L] (X = CN, NCO, *or* N_3). The cyano-, isocyanato-, and azido-iron(III) complexes were obtained by mixing [Fe(Cl)L] and the corresponding sodium or potassium salts of the ligands X. The synthesis of the azido-complex $[Fe(N_3)L]$ is exemplified. To a solution of [Fe(Cl)L] (2.143 g, 5 mmol) in methanol (50 cm^3) was added a solution of NaN_3 (0.455 g, 7 mmol) in the minimum amount of water. The mixture was warmed at 50 °C on a water-bath for 10 min and the solution filtered. The filtrate was stood overnight to precipitate black crystals. They were collected, washed with methanol and diethyl ether, and dried *in vacuo*.

Complexes $[Fe(X)L]BPh_4$ (X = py, apy, 3Me-py, 4Me-py, 3,4Me_2-py, Him, 2Me-im, *or* mim). The iron(III) complexes with pyridine, imidazole, and their derivatives were obtained by mixing [Fe(Cl)L] with the appropriate base; tetraphenylborate was used as counter anion. The synthesis of the pyridine complex $[Fe(py)L]BPh_4$ is exemplified in detail. To a solution of [Fe(Cl)L] (0.857 g, 2 mmol) in methanol (50 cm^3) was added an excess of pyridine (0.237 g, 3 mmol). The mixture was warmed at 60 °C for 30 min and then filtered. The filtrate was added to a solution of sodium tetraphenylborate (0.684 g, 2 mmol) in methanol (10 cm^3). The mixture was warmed at 60 °C for 5 min and stood overnight to precipitate black crystals. They were collected, washed with methanol and diethyl ether, and dried *in vacuo*.

Physical Measurements.—Melting points were measured on a Yanagimoto micromelting points apparatus and were uncorrected. Elemental analyses were performed by Mr. Shinichi Miyazaki at the Technical Service Centre of Kumamoto University. Electrical conductivity measurements were carried out on a Denki Kagaku AOC-10 apparatus in dichloromethane solution on *ca.* 10^{-3} mol dm^{-3} solutions. Thermal analyses (t.g., d.t.a.) were performed on a Rigaku Denki 8113RH thermal analyzer, in order to detect the solvent molecule of crystallization. The measurements were carried out under an argon atmosphere, at a heating rate of 5 °C min^{-1}, using *ca.* 10 mg of the sample for each run. I.r. spectra were recorded as KBr discs with a Shimadzu IR 410 spectrophotometer. The temperature dependence of the electronic spectra in dichloromethane solution was recorded with a Hitachi 340 spectrophotometer, in the temperature range 240—280 K, according to a literature procedure.[8]

Magnetic susceptibilities were measured by the Faraday method in the range from liquid nitrogen temperature to room temperature, according to the procedure reported earlier.[9] The susceptibility was corrected for the diamagnetism of the component atoms using Pascal's constants. The effective magnetic moments were calculated by using the equation $\mu_{eff.} = 2.828\sqrt{\chi_A T}$, where χ_A is the magnetic susceptibility per mole of iron atoms.

Differential scanning calorimetry (d.s.c.) was carried out with a Rigaku Denki DSC 8230 apparatus. The sample temperature was varied between 150 and 400 K at a constant heating rate of 5 °C min^{-1}. The sensitivity of the instrument was 0.25 mcal s^{-1}, and α-Al_2O_3 was used as reference sample. The sample was packed into an aluminium pan and then sealed.

Mössbauer spectra were recorded on a conventional Austin Science apparatus driven in constant-acceleration mode.[10] All isomer shifts are reported with respect to the centroid of the spectrum of an iron foil enriched with ^{57}Fe at 295 K, which was also used as a standard material for velocity calibration.

X-*Ray Diffraction Analysis of* $[Fe(4Me\text{-}py)L]BPh_4$.—Black rhombic crystals were obtained by slow precipitation from a methanol solution at room temperature. A crystal with approximate dimensions 0.5 × 0.4 × 0.6 mm was used for the *X*-ray diffraction study. Diffraction data were obtained on a Rigaku AFC-5 four-circle diffractometer at the Faculty of Science, Kyushu University, using graphite-monochromatized Mo-K_α radiation (λ = 0.710 73 Å) at 20 ± 1 °C. Lattice parameters and their estimated standard deviations were obtained from a least-squares fit to 25 2θ values in the range $15 < 2\theta < 30°$.

Crystal data. $C_{50}H_{50}BFeN_4O_2$, M = 805.6, monoclinic, a = 20.884(3), b = 16.715(6), c = 12.456(2) Å, β = 96.62(1)°, U = 4 319.0(20) Å^3, D_m = 1.215 g cm^{-3}, Z = 4, D_c = 1.240 g cm^{-3}, space group $P2_1/a$, $F(000)$ = 1 700, μ = 4.1 cm^{-1}.

For the intensity data collection, the θ–2θ scan mode was used at a scan rate of 4° min^{-1}. Three standard reflections were monitored every 100 reflections and their intensities showed a good stability (< 3% change). A total of 4 416 reflections were collected in the range $1.5 < 2\theta < 48°$, of which 3 841 independent reflections with $|F_o| > 3\sigma(|F_o|)$ were used for the structure determination. The intensity data were corrected for Lorentz-polarization effects, but not for absorption.

Solution and refinement of the structure. All the calculations were carried out on the FACOM M-200 computer at the Computer Centre of Kyushu University with the universal crystallographic computation program system UNICS III.[11] Atomic scattering factors for non-hydrogen atoms were taken from ref. 12 and those for hydrogen from Stewart *et al.*[13] The effects of anomalous dispersion for non-hydrogen atoms were corrected for in the structure factor calculations.

The structure was solved by the heavy-atom method and refined by block-diagonal least-squares techniques. The position of the iron atom was determined from a three-dimensional Patterson function, and successive Fourier syntheses located all the non-hydrogen atoms. Anisotropic thermal parameters were introduced for all the non-hydrogen atoms. Further difference Fourier syntheses located all the hydrogen atoms and their positional and isotropic thermal parameters were refined. Reliability factors are defined as $R = \Sigma||F_o| - |F_c||/\Sigma|F_o|$ and $R' = [\Sigma w(|F_o| - |F_c|)^2/\Sigma w|F_o|^2]^{\frac{1}{2}}$, where the weights were taken as $w = 1/\sigma(F_o)^2$. The final values of R and R' were 0.0763 and 0.0773, respectively. Final positional parameters with their estimated standard deviations are given in Table 1.

Table 1. Atomic co-ordinates ($\times 10^4$) and isotropic thermal parameters* for $[Fe(4Me\text{-}py)L]BPh_4$

Atom	x	y	z	$B_{equiv.}$	Atom	x	y	z	$B_{equiv.}$
Fe	1 167(1)	2 117(1)	3 019(1)	3.71(3)	C(23)	2 153(5)	349(7)	655(8)	6.89(35)
O(1)	571(3)	1 302(3)	3 245(4)	4.82(17)	C(24)	2 079(4)	1 138(7)	412(7)	6.45(34)
O(2)	1 750(3)	2 928(3)	2 737(5)	5.13(18)	C(25)	1 799(4)	1 655(6)	1 127(7)	5.22(29)
N(1)	551(3)	2 529(4)	1 808(5)	5.05(22)	C(26)	2 437(7)	−228(9)	−93(11)	10.93(54)
N(2)	759(3)	2 878(5)	4 021(6)	5.69(24)	B	4 156(5)	1 678(6)	7 587(8)	4.18(30)
N(3)	1 770(3)	1 754(4)	4 274(5)	4.54(21)	C(27)	4 957(4)	1 761(5)	7 762(6)	3.97(24)
N(4)	1 583(3)	1 382(4)	2 026(5)	4.14(20)	C(28)	5 378(4)	1 156(5)	7 557(7)	4.99(28)
C(1)	196(4)	940(5)	2 489(7)	4.37(26)	C(29)	6 049(5)	1 218(6)	7 841(8)	6.01(32)
C(2)	−27(5)	162(6)	2 675(9)	6.62(35)	C(30)	6 298(4)	1 914(6)	8 371(8)	6.28(33)
C(3)	−416(5)	−252(6)	1 926(10)	8.22(42)	C(31)	5 899(4)	2 517(6)	8 599(7)	5.64(29)
C(4)	−597(5)	81(7)	924(10)	8.26(41)	C(32)	5 242(4)	2 419(5)	8 313(6)	4.56(25)
C(5)	−424(4)	847(7)	697(8)	6.37(34)	C(33)	3 899(4)	991(5)	6 706(6)	4.30(25)
C(6)	−17(4)	1 296(6)	1 470(7)	4.78(27)	C(34)	4 172(5)	868(6)	5 736(7)	5.52(30)
C(7)	117(4)	2 102(6)	1 255(7)	4.99(28)	C(35)	3 910(6)	373(8)	4 945(8)	8.42(43)
C(8)	556(5)	3 381(6)	1 574(9)	7.06(37)	C(36)	3 370(6)	−81(7)	5 084(9)	8.05(40)
C(9)	430(5)	3 835(6)	2 516(10)	8.43(41)	C(37)	3 081(5)	7(6)	6 023(8)	6.64(34)
C(10)	340(8)	3 518(8)	3 455(13)	12.27(63)	C(38)	3 342(4)	530(5)	6 810(7)	4.82(27)
C(11)	658(8)	2 589(8)	4 981(10)	11.24(57)	C(39)	3 831(4)	2 499(5)	7 046(6)	4.50(24)
C(12)	1 076(5)	2 079(11)	5 655(8)	11.60(61)	C(40)	4 143(5)	3 067(6)	6 468(7)	5.69(30)
C(13)	1 473(5)	1 398(7)	5 200(7)	7.30(38)	C(41)	3 842(5)	3 720(6)	5 929(9)	7.20(36)
C(14)	2 389(4)	1 894(6)	4 387(7)	5.11(28)	C(42)	3 193(6)	3 820(7)	5 978(10)	8.82(43)
C(15)	2 710(4)	2 371(5)	3 687(6)	4.25(25)	C(43)	2 849(5)	3 300(7)	6 530(10)	8.14(40)
C(16)	3 397(5)	2 425(7)	3 844(7)	6.73(34)	C(44)	3 158(5)	2 641(6)	7 065(8)	6.69(34)
C(17)	3 724(4)	2 958(8)	3 281(8)	7.71(39)	C(45)	3 975(4)	1 487(5)	8 797(6)	4.29(25)
C(18)	3 393(5)	3 490(6)	2 580(8)	6.03(32)	C(46)	4 144(5)	757(6)	9 262(7)	5.77(31)
C(19)	2 739(4)	3 458(6)	2 406(8)	5.81(31)	C(47)	4 058(5)	548(7)	10 326(8)	7.64(39)
C(20)	2 388(4)	2 915(5)	2 936(6)	4.31(25)	C(48)	3 799(5)	1 112(9)	10 927(8)	9.01(46)
C(21)	1 663(5)	596(6)	2 280(7)	5.68(31)	C(49)	3 610(5)	1 860(8)	10 522(9)	8.40(42)
C(22)	1 944(5)	67(6)	1 597(9)	7.33(37)	C(50)	3 719(4)	2 017(7)	9 474(8)	6.27(33)

* $B_{equiv.} = \frac{4}{3}(\beta_{11}a^2 + \beta_{22}b^2 + \beta_{33}c^2 + \beta_{13}ac\cos\beta)$.

Table 2. Elemental analyses[a] (%), melting points, colours at *ca.* 80 and 300 K in the solid state, and electrical conductivities

Complex	H	C	N	M.p.(°C)	Colour[b] 300	Colour[b] 80	Λ[c]
$[Fe(Cl)L]\cdot CH_3OH$	5.60 (5.90)	54.85 (54.75)	9.45 (9.10)	>300	V	V	0.0
$[Fe(CN)L]\cdot 1.5CH_3OH$	6.10 (6.25)	57.50 (57.85)	12.25 (12.00)	>300	G	G	0.0
$[Fe(N_3)L]\cdot 0.5H_2O$	5.40 (5.45)	53.70 (54.05)	18.70 (18.90)	>300	V	V	0.0
$[Fe(NCO)L]\cdot 0.5H_2O$	5.40 (5.45)	56.75 (56.75)	12.35 (12.60)	>300	V	V	0.0
$[Fe(Him)L]BPh_4$	6.05 (6.05)	72.00 (72.30)	8.80 (8.95)	182—184	V	V	47.7
$[Fe(2Me\text{-}im)L]BPh_4$	6.15 (6.20)	72.20 (72.55)	8.75 (8.80)	206—209	V	G	51.9
$[Fe(mim)L]BPh_4$	6.25 (6.20)	72.10 (72.55)	8.60 (8.80)	172—175	V	V	55.6
$[Fe(py)L]BPh_4$	6.10 (6.10)	74.15 (74.35)	7.00 (7.10)	163—164	B	G	44.5
$[Fe(3Me\text{-}py)L]BPh_4$	6.30 (6.25)	74.30 (74.55)	6.80 (6.95)	158—160	DV	C	53.0
$[Fe(4Me\text{-}py)L]BPh_4$	6.20 (6.25)	74.55 (74.55)	6.95 (6.95)	161—162	DV	G	52.9
$[Fe(3,4Me_2\text{-}py)L]BPh_4$	6.40 (6.40)	74.55 (74.75)	6.80 (6.85)	169—172	B	G	54.3
$[Fe(apy)L]BPh_4$	6.10 (6.00)	72.95 (73.05)	8.50 (8.70)	185—188	V	G	50.6

[a] Calculated values are given in parentheses. [b] V = violet, G = green, B = black, DV = dark violet, DG = dark green. [c] Electrical conductivity (S cm^2 mol^{-1}).

Results and Discussion

In this study, iron(III) complexes of general formula $[Fe(X)L]^{n+}$ (n = 0 or 1) were prepared, where L is a quinquedentate ligand derived from salicylaldehyde and di(3-aminopropyl)amine, and X is a unidentate ligand (see Figure 1). The chloro-iron(III) complex [Fe(Cl)L] was used as the starting material for the preparation of the other complexes. The chloro-ligand was easily substituted by ligands having a stronger ligand field to give the substituted complexes. For the iron(III) complexes containing a unidentate neutral ligand, tetraphenylborate was used as counter anion.

Analytical data, melting points, the colours at room temperature and liquid nitrogen temperature in the solid state, and the molar electrical conductances are given in Table 2. Some of the complexes tend to crystallize as solvates. The crystal solvents were detected by thermal analysis, where weight losses corresponding to the fraction of solvent molecule estimated by elemental analysis were observed. Electrical conductances agree with the complexes containing a mono-anionic unidentate ligand (X = Cl, N_3, NCO, or CN^-) being neutral, and those containing a neutral unidentate ligand being monocationic (X = py, apy, 3Me-py, 4Me-py, $3,4Me_2$-py, Him, 2Me-im, or mim), indicating that the series of iron(III) complexes are six-co-ordinated (N_3O_2 donors of the dianionic quinquedentate ligand and a monoanionic or neutral unidentate ligand X).

The co-ordination of cyano-, isocyanato-, and azido-ion to iron(III) can be also identified by the specific i.r. bands of these

Table 3. Magnetic data ($\mu_{eff.}$/B.M.) at *ca.* 80 and 300 K*

Complex	$\mu_{eff.}$ (*T*/K)	$\mu_{eff.}$ (*T*/K)
[Fe(Cl)L]	5.80 (86.9)	5.82 (297.6)
[Fe(N_3)L]	6.00 (99.9)	5.98 (294.7)
[Fe(mim)L]BPh_4	5.75 (86.9)	5.86 (297.6)
[Fe(Him)L]BPh_4	5.96 (79.0)	5.95 (294.0)
[Fe(2Me-im)L]BPh_4	2.32 (78.8)	5.50 (300.0)
[Fe(3Me-py)L]BPh_4	2.18 (86.9)	4.39 (297.4)
[Fe(py)L]BPh_4	2.08 (87.4)	4.18 (296.9)
[Fe(3,4Me_2-py)L]BPh_4	2.31 (78.0)	4.10 (305.0)
[Fe(4Me-py)L]BPh_4	2.26 (80.0)	3.54 (300.0)
[Fe(CN)L]	2.12 (86.9)	2.49 (293.0)

* Temperature is given in parentheses.

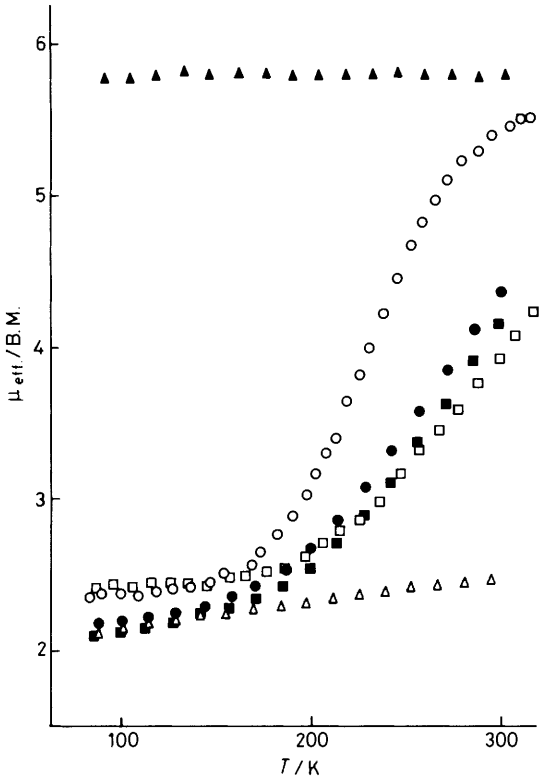

Figure 2. Temperature dependence of the effective magnetic moments ($\mu_{eff.}$) for [Fe(Cl)L] (▲), [Fe(CN)L] (△), [Fe(py)L]BPh_4 (■), [Fe(3Me-py)L]BPh_4 (●), [Fe(3,4Me_2-py)L]BPh_4 (□), and [Fe(2Me-im)L]BPh_4 (○)

anions, since it is well known that the specific bands shift to higher frequencies upon co-ordination to a metal.[13] The chloro-iron(III) complex [Fe(Cl)L] exhibits no band in the region 2 000—2 300 cm^{-1}. The iron(III) complexes [Fe(CN)L], [Fe(NCO)L], and [Fe(N_3)L] each exhibit a sharp i.r. absorption band at 2 130, 2 200, and 2 065 cm^{-1}, respectively, attributable to ν(CN), ν_{asym}(NCO), and ν_{asym}(NNN), respectively. Each band is located at a higher frequency compared with that of the corresponding free ion.[14]

Magnetic Properties.—The preliminary observation of thermochromism in the solid state shown in Table 1 suggested a spin equilibrium, and the temperature dependence of the magnetic properties was examined; data at *ca.* 80 and 300 K are summarized in Table 3. The temperature dependence of the

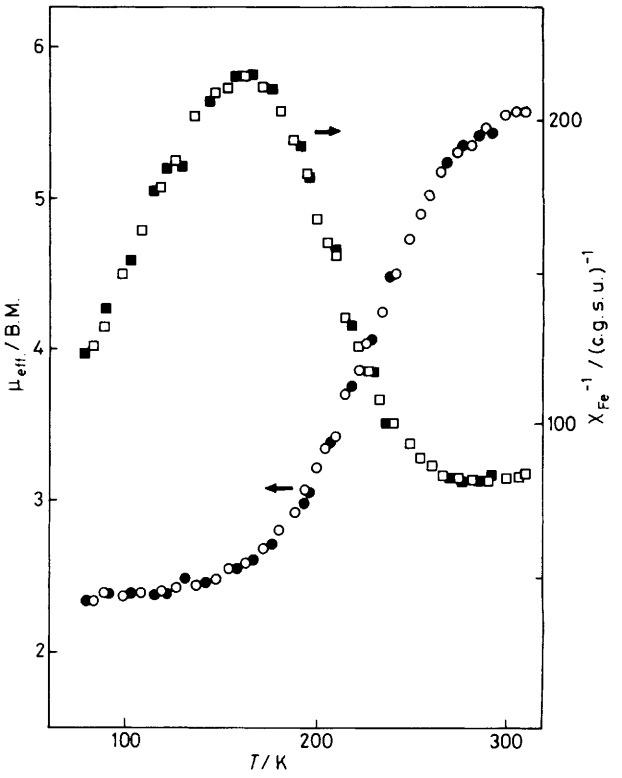

Figure 3. Temperature dependence of the effective magnetic moments ($\mu_{eff.}$) for [Fe(2Me-im)L]BPh_4, along with the plot of $1/\chi_A$ *vs.* temperature: (○, □) increasing temperature sequence, (●, ■) decreasing temperature sequence

magnetic moments for some of the complexes are shown in Figure 2. The magnetic moments of [Fe(Cl)L], [Fe(N_3)L], [Fe(Him)L]BPh_4, and [Fe(mim)L]BPh_4 are typical values of high-spin ($S = \frac{5}{2}$) over the temperature range studied;[15] [Fe(CN)L] is essentially low-spin ($S = \frac{1}{2}$).[15] On the other hand, the effective magnetic moments of [Fe(py)L]BPh_4, [Fe(3Me-py)L]BPh_4, [Fe(4Me-py)L]BPh_4, [Fe(3,4Me_2-py)L]BPh_4, and [Fe(2Me-im)L]BPh_4 increase gradually from *ca.* 2.1 B.M. at 80 K, with increase of the temperature, exhibiting spin-equilibrium behaviour ($S = \frac{5}{2} \rightleftarrows S = \frac{1}{2}$). Since in the present series of complexes $[Fe(X)L]^{n+}$ ($n = 0$ or 1), the quinquedentate ligand L is kept constant, the difference in the averaged ligand field strength among the complexes depends on that of X. According to the Tanabe–Sugano diagram for the d^5 electronic configuration in an octahedral ligand field, the ground state changes from ^6A to ^2T at cross-over point, when the ligand field strength increases. Therefore, it is expected that the ground state, *i.e.* the spin state, for the present series of iron(III) complexes depends on the ligand field strength of X. As the order of the spectrochemical series is CN > pyridine or imidazole derivatives > N_3 > Cl, the magnetic behaviour for the complexes is well consistent with the spectrochemical series (ligand field strength) of X.

The temperature dependences of the effective magnetic moments and $1/\chi_A$ for [Fe(2Me-im)L]BPh_4 are shown in Figure 3 for both increasing- and decreasing-temperature sequences. The plot of $1/\chi_A$ *vs.* *T* exhibits non-Curie behaviour giving evidence of a spin transition. The effective magnetic moment changes gradually from 2.3 B.M. at 80 K to 5.5 B.M. at 300 K. The magnetic behaviour for the increasing- and decreasing-temperature sequences is practically the same, indicating that the spin transition between high-spin and low-

Table 4. Mössbauer parameters for $[Fe(2Me\text{-}im)L]BPh_4$

Temp. (K)	δ^a	Δ^a	$\Gamma(l)^{a,b}$	$\Gamma(u)^{a,b}$	$I(l)^c$	$I(u)^c$	$A(l)^d$	$A(u)^d$	χ^2/Freedom^e
78	0.284	2.716	1.093	1.201	0.038 66	0.031 01	3.404	3.002	750/493
120	0.269	2.621	0.723	0.985	0.044 73	0.032 81	2.605	2.604	602/493
150	0.252	2.491	0.556	0.671	0.044 45	0.038 26	1.989	2.067	685/493
203	0.264	2.052	0.982	0.842	0.020 14	0.022 15	1.593	1.503	816/493
225	0.317	1.645	1.323	1.021	0.013 81	0.014 92	1.472	1.227	567/493
250	0.366	1.241	1.285	1.117	0.010 42	0.009 39	1.078	0.844	458/493
273	0.344	1.043	1.017	1.247	0.008 78	0.006 84	0.720	0.687	516/493
298	0.325	1.003	0.893	1.444	0.007 42	0.005 48	0.533	0.367	513/493
Analysis as two doublets									
150	0.549	1.209	1.757	1.757	0.002 84	0.002 84	0.403	0.403^f	450/489
	0.255	2.515	0.506	0.574	0.044 35	0.036 87	1.807	1.705	
203	0.447	1.298	1.384	1.384	0.005 80	0.005 80	0.646	0.646^f	552/489
	0.246	2.194	0.651	0.555	0.018 20	0.018 05	0.954	0.807	

^{a} Units are mm s^{-1}. ^{b} Full width at half maximum (f.w.h.m.); l = lower energy peak, u = upper energy peak. ^{c} Peak intensity. ^{d} Area under the absorption curve. ^{e} Sum of the squares of the weighted residuals. ^{f} Some constraints are required to analyze this doublet.

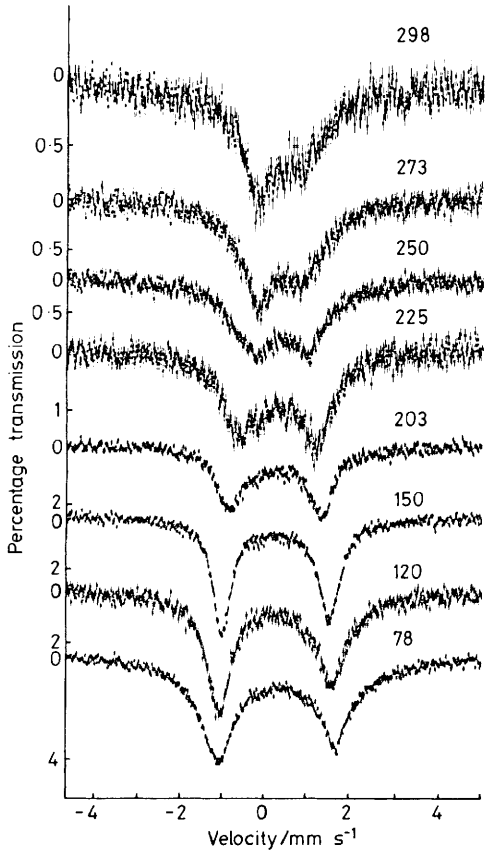

Figure 4. Temperature dependence (K) of the Mössbauer spectra of $[Fe(2Me\text{-}im)L]BPh_4$

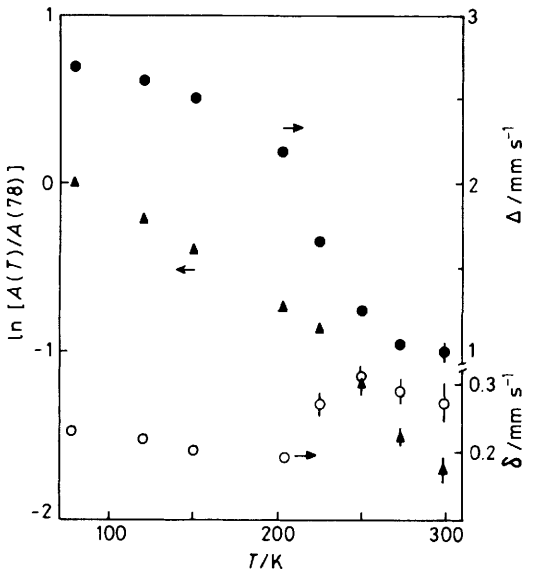

Figure 5. Temperature dependence of the isomer shift (○), quadrupole splitting (●), and area under the Mössbauer resonance line, ln $[A(T)/A(78)]$, (▲) for $[Fe(2Me\text{-}im)L]BPh_4$

spin states is not associated with a thermal hysteresis. These results imply that the complex is classified as a continuous type of high-spin $\rightleftarrows$ low-spin transition, on the basis of the criterion of König *et al.*[16]

Mössbauer Spectra.—The Mössbauer spectra for $[Fe(2Me\text{-}im)L]BPh_4$ at various temperatures are shown in Figure 4. The Mössbauer parameters derived from the spectra are given in Table 4. The spectra were initially analyzed to a single doublet; spectra typical for low-spin iron(III) are observed below 150 K. On the other hand, absorptions for high-spin iron(III) are observed in the spectra at 298 K in accordance with the magnetic susceptibility data. The spectra below 203 K are not reliably analyzed, as shown in the χ^2 values in Table 4 by which the goodness of fit is monitored. Then, the spectra at 150 and 203 K were analyzed as two doublets, of high- and low-spin isomers. The population (x) of high-spin isomer at a certain temperature is obtained by assuming simple additive properties for magnetic susceptibilities. The values of x are 0.06 at 150 K and 0.22 at 203 K, if μ_h = 5.90 B.M. and μ_l = 2.00 B.M. are assumed. However, these values are not in accordance with the values evaluated from the Mössbauer absorption area, based on the assumption that high- and low-spin isomers have the same recoil-free fraction, although it seems likely that it is less for the former than for the latter isomer.[17] Furthermore, quadrupole splitting values (Δ) for high-spin isomers appear too large compared with the normal values for high-spin iron(III) complexes; that analyzing the Mössbauer spectra as two doublets is inappropriate is shown by this discrepancy.

The temperature for the equi-existence of high- and low-spin isomers is evaluated to be 233 K from the magnetic data. However, the spectra at 225 and 250 K can be analyzed as a single doublet with good reliabilities of $\chi^2 = 567$ at 225 K and $\chi^2 = 458$ at 250 K. If the spectra are analyzed as a single doublet, the plots shown in Figure 5 are explained as follows (error bars represent statistical errors only). The Δ values decrease on increasing the temperature and markedly in the temperature range 180—260 K. The temperature dependence of the isomer shift (δ) exhibits the typical behaviour of a low-spin or high-spin iron(III) state below 180 K or above 260 K, respectively, since it is expected that δ values decrease with increasing temperature for spin-invariant complexes due to the temperature dependence of the second-order Doppler shift. However, in the temperature range 180—260 K, the values increase drastically according to the increase of the population of high-spin state (or isomer) in accordance with the decrease of Δ values.

The spectra for rapid intercrossing between high- and low-spin states have been theoretically examined by Maeda and Takashima.[18] It is expected that the relaxation spectra with the end components (the spectra for high- or low-spin isomers) of an antisymmetric doublet could not be reliably analyzed, and

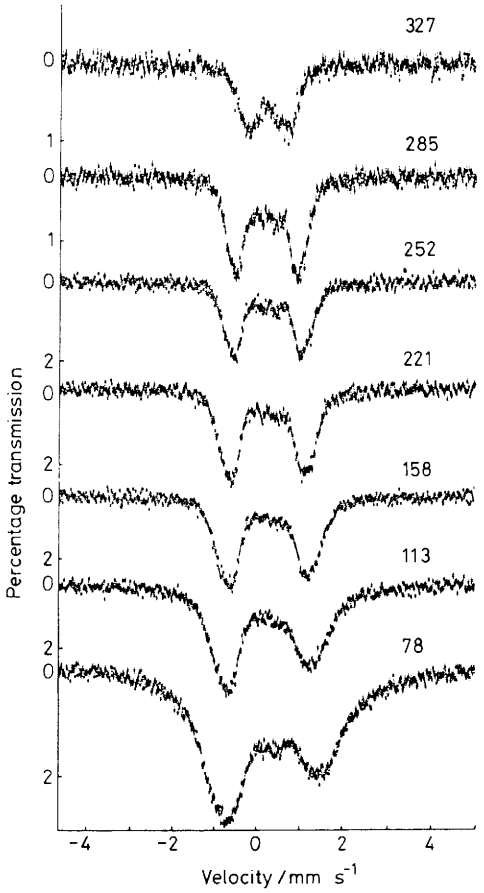

Figure 6. Temperature dependence (K) of the Mössbauer spectra of $[Fe(4Me\text{-}py)L]BPh_4$

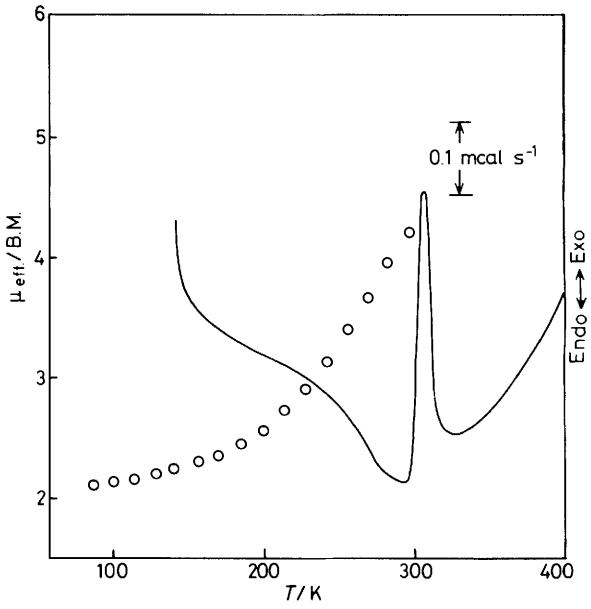

Figure 7. D.s.c. curve for $[Fe(py)L]BPh_4$ for increasing temperature sequence, along with the temperature dependence of the magnetic moments

Table 5. Bond distances (Å) for $[Fe(4Me\text{-}py)L]BPh_4$ with estimated standard deviations in parentheses

(*a*) Cation							
Fe–O(1)	1.887(5)	N(2)–C(10)	1.505(16)	C(4)–C(5)	1.368(16)	C(16)–C(17)	1.364(15)
Fe–O(2)	1.882(5)	N(2)–C(11)	1.329(15)	C(5)–C(6)	1.422(12)	C(17)–C(18)	1.375(14)
Fe–N(1)	1.987(6)	N(3)–C(13)	1.494(12)	C(6)–C(7)	1.408(13)	C(18)–C(19)	1.360(13)
Fe–N(2)	2.035(7)	N(3)–C(14)	1.305(11)	C(8)–C(9)	1.447(16)	C(19)–C(20)	1.380(12)
Fe–N(3)	1.986(6)	N(4)–C(21)	1.356(11)	C(9)–C(10)	1.317(20)	C(21)–C(22)	1.400(14)
Fe–N(4)	2.010(6)	N(4)–C(25)	1.335(11)	C(11)–C(12)	1.423(19)	C(22)–C(23)	1.380(15)
O(1)–C(1)	1.303(9)	C(1)–C(2)	1.409(13)	C(12)–C(13)	1.553(19)	C(23)–C(24)	1.358(16)
O(2)–C(20)	1.327(9)	C(1)–C(6)	1.424(11)	C(14)–C(15)	1.407(12)	C(23)–C(26)	1.509(18)
N(1)–C(7)	1.288(10)	C(2)–C(3)	1.354(15)	C(15)–C(16)	1.427(12)	C(24)–C(25)	1.414(13)
N(1)–C(8)	1.454(12)	C(3)–C(4)	1.379(16)	C(15)–C(20)	1.417(11)		
(*b*) Anion							
B–C(27)	1.667(12)	C(29)–C(30)	1.408(13)	C(36)–C(37)	1.384(15)	C(43)–C(44)	1.405(14)
B–C(33)	1.635(12)	C(30)–C(31)	1.359(14)	C(37)–C(38)	1.377(12)	C(45)–C(46)	1.379(12)
B–C(39)	1.642(13)	C(31)–C(32)	1.387(12)	C(39)–C(40)	1.397(12)	C(45)–C(50)	1.373(13)
B–C(45)	1.626(12)	C(33)–C(34)	1.408(12)	C(39)–C(44)	1.428(13)	C(46)–C(47)	1.401(13)
C(27)–C(28)	1.383(12)	C(33)–C(38)	1.414(12)	C(40)–C(41)	1.392(13)	C(47)–C(48)	1.355(17)
C(27)–C(32)	1.392(11)	C(34)–C(35)	1.352(14)	C(41)–C(42)	1.374(16)	C(48)–C(49)	1.388(18)
C(28)–C(29)	1.408(12)	C(35)–C(36)	1.387(17)	C(42)–C(43)	1.362(17)	C(49)–C(50)	1.376(14)

then the interconversion rate for this complex could not be calculated from the spectra. However, it should be noted that in the intermediate temperature ranges for coexistence of high- and low-spin isomers, only one doublet is observed in the Mössbauer spectra, and that the interconversion rate between high- and low-spin states (the rate of electronic relaxation of spin transition) is comparable with the inverse of the lifetime of the excited Mössbauer nuclear state (1×10^{-7} s); the nucleus sees an 'average' of the high- and low-spin electronic states. Although the rates of spin-interexchange at 225 and 250 K are a little slower than 10^7 s^{-1}, the rates are of this order on increasing the temperature.

The spectrum at 78 K is very broad and the reason is not clear; however, spin–spin or spin–lattice relaxation effects on $^2T_2$ may be induced, because of the presence of the bulky anion BPh_4^- and the large Fe ••• Fe distance.

The temperature dependence of a recoil-free fraction (f) is given by the absorption area under the resonance curves. The Debye model approximation in the high-temperature limit leads to the hypothesis, $d \ln f/dT \propto d \ln A/dT$, where A is a normalized absorption area. The plot of $\ln [A(T)/A(78)]$ is shown in Figure 5; the temperature dependence shows no discontinuity in the curve, suggesting the absence of a change in the crystal lattice. The slope of $\ln [A[T)/A(78)]$ *vs.* T with rising temperature shows that the recoil-free fraction of the high-spin isomer is smaller than that of the low-spin isomer.

The temperature dependence of the Mössbauer spectra for $[Fe(4Me\text{-}py)L]BPh_4$ is shown in Figure 6. At the highest temperature studied (327 K), the spectrum consists of a single doublet characterized by $\Delta = 0.847$ mm s^{-1} with $\delta = 0.214$ mm s^{-1}, although the values of f.w.h.m. are considerably large compared with the natural linewidth of 0.195 mm s^{-1}. Values of

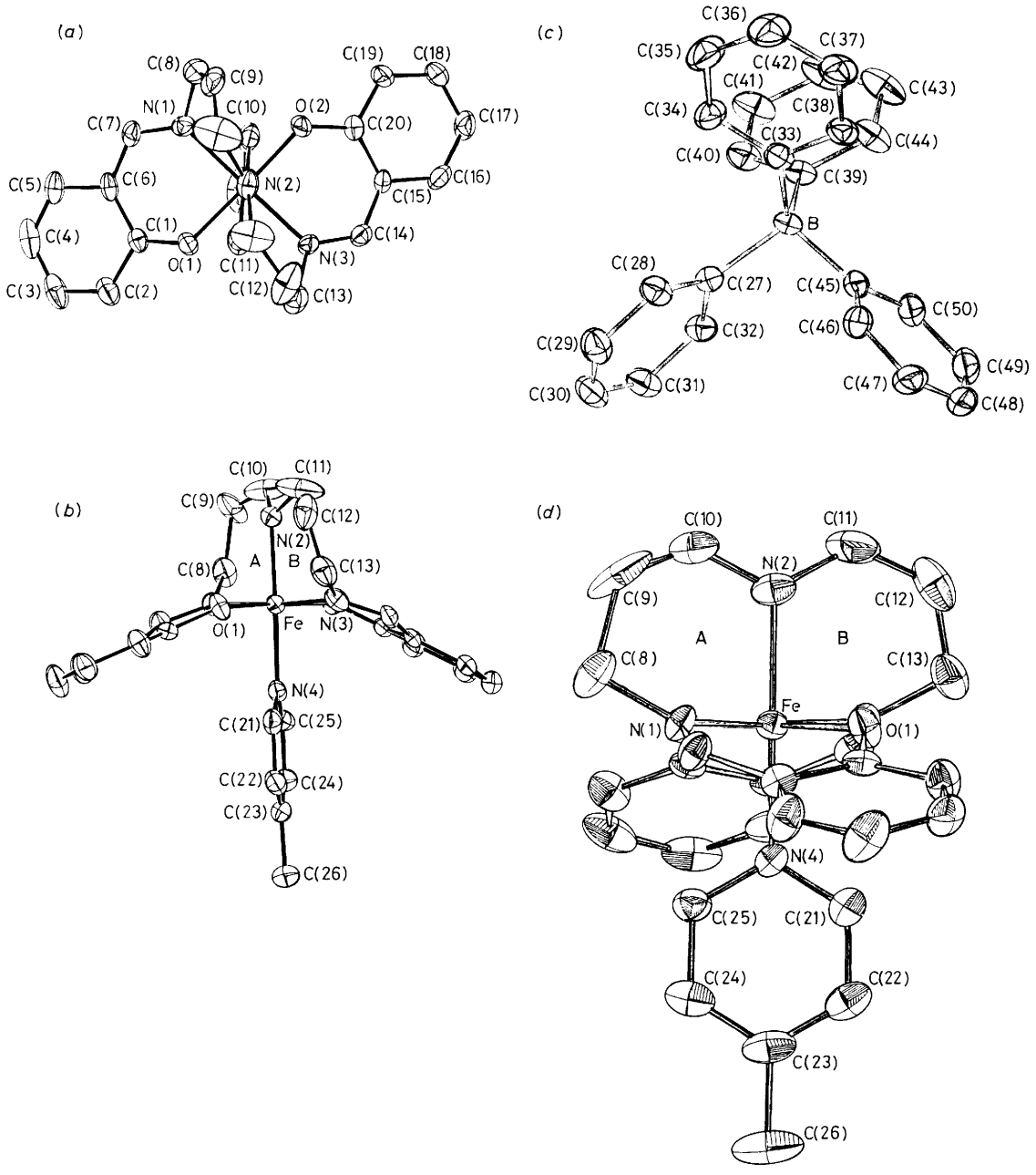

Figure 8. Perspective drawings of $[Fe(4Me\text{-}py)L]BPh_4$ with the atom numbering scheme

Table 6. Bond angles (°) for [Fe(4Me-py)L]BPh_4 with estimated standard deviations in parentheses

(*a*) Cation

O(1)–Fe–O(2)	177.8(2)	C(10)–N(2)–C(11)	122.3(10)	N(2)–C(11)–C(12)	126.7(13)
O(1)–Fe–N(1)	89.0(2)	Fe–N(3)–C(13)	116.5(5)	C(11)–C(12)–C(13)	122.7(9)
O(1)–Fe–N(2)	91.7(2)	Fe–N(3)–C(14)	124.1(5)	N(3)–C(13)–C(12)	106.0(9)
O(1)–Fe–N(3)	91.7(2)	C(13)–N(3)–C(14)	118.8(6)	N(3)–C(14)–C(15)	124.8(7)
O(1)–Fe–N(4)	89.4(2)	Fe–N(4)–C(21)	119.9(5)	C(14)–C(15)–C(16)	119.6(7)
O(2)–Fe–N(1)	89.1(2)	Fe–N(4)–C(25)	121.2(5)	C(14)–C(15)–C(20)	123.2(7)
O(2)–Fe–N(2)	89.3(2)	C(21)–N(4)–C(25)	118.7(7)	C(16)–C(15)–C(20)	116.2(7)
O(2)–Fe–N(3)	90.1(2)	O(1)–C(1)–C(2)	119.4(7)	C(15)–C(16)–C(17)	121.6(8)
O(2)–Fe–N(4)	89.4(2)	O(1)–C(1)–C(6)	123.3(7)	C(16)–C(17)–C(18)	120.2(8)
N(1)–Fe–N(2)	88.2(2)	C(2)–C(1)–C(6)	117.1(7)	C(17)–C(18)–C(19)	119.8(9)
N(1)–Fe–N(3)	177.0(3)	C(1)–C(2)–C(3)	122.7(9)	C(18)–C(19)–C(20)	121.9(8)
N(1)–Fe–N(4)	91.8(2)	C(2)–C(3)–C(4)	119.8(10)	O(2)–C(20)–C(15)	121.6(7)
N(2)–Fe–N(3)	88.8(2)	C(3)–C(4)–C(5)	120.8(9)	O(2)–C(20)–C(19)	118.4(7)
N(2)–Fe–N(4)	178.8(2)	C(4)–C(5)–C(6)	120.3(9)	C(15)–C(20)–C(19)	119.9(7)
N(3)–Fe–N(4)	90.9(2)	C(1)–C(6)–C(5)	118.8(8)	N(4)–C(21)–C(22)	121.2(8)
Fe–O(1)–C(1)	125.4(5)	C(1)–C(6)–C(7)	121.3(7)	C(21)–C(22)–C(23)	119.7(9)
Fe–O(2)–C(20)	127.5(5)	C(5)–C(6)–C(7)	119.4(7)	C(22)–C(23)–C(24)	118.7(9)
Fe–N(1)–C(7)	124.5(6)	N(1)–C(7)–C(6)	124.8(7)	C(22)–C(23)–C(26)	119.5(10)
Fe–N(1)–C(8)	118.1(5)	N(1)–C(8)–C(9)	110.1(9)	C(24)–C(23)–C(26)	121.6(10)
C(7)–N(1)–C(8)	117.0(7)	C(8)–C(9)–C(10)	124.5(10)	C(23)–C(24)–C(25)	119.8(9)
Fe–N(2)–C(10)	114.7(7)	N(2)–C(10)–C(9)	124.4(13)	N(4)–C(25)–C(24)	121.5(8)
Fe–N(2)–C(11)	116.4(7)				

(*b*) Anion

C(27)–B–C(33)	113.1(7)	C(27)–C(32)–C(31)	125.0(8)	C(40)–C(41)–C(42)	117.8(10)
C(27)–B–C(39)	110.1(7)	B–C(33)–C(34)	123.0(7)	C(41)–C(42)–C(43)	121.6(10)
C(27)–B–C(45)	103.4(6)	B–C(33)–C(38)	122.0(7)	C(42)–C(43)–C(44)	119.9(10)
C(33)–B–C(39)	102.8(6)	C(34)–C(33)–C(38)	114.6(7)	C(39)–C(44)–C(43)	121.3(9)
C(33)–B–C(45)	113.0(7)	C(33)–C(34)–C(35)	123.0(9)	B–C(45)–C(46)	119.1(7)
C(39)–B–C(45)	114.5(7)	C(34)–C(35)–C(36)	120.6(10)	B–C(45)–C(50)	126.2(8)
B–C(27)–C(28)	124.3(7)	C(35)–C(36)–C(37)	119.1(10)	C(46)–C(45)–C(50)	114.3(8)
B–C(27)–C(32)	119.6(7)	C(36)–C(37)–C(38)	119.5(9)	C(45)–C(46)–C(47)	124.2(9)
C(28)–C(27)–C(32)	115.0(7)	C(33)–C(38)–C(37)	122.8(8)	C(46)–C(47)–C(48)	116.9(10)
C(27)–C(28)–C(29)	122.3(8)	B–C(39)–C(40)	125.7(7)	C(47)–C(48)–C(49)	122.6(10)
C(28)–C(29)–C(30)	118.8(8)	B–C(39)–C(44)	119.5(7)	C(48)–C(49)–C(50)	116.4(10)
C(29)–C(30)–C(31)	120.5(8)	C(40)–C(39)–C(44)	114.5(8)	C(45)–C(50)–C(49)	125.3(10)
C(30)–C(31)–C(32)	118.1(8)	C(39)–C(40)–C(41)	124.6(9)		

δ in the case where the spectra are analyzed as a doublet are 0.309 (78), 0.263 (113), 0.244 (158), 0.225 (221), 0.217 (252), 0.208 (285), and 0.214 mm s^{-1} (327 K). The increase of δ at 327 K supports the fact that the rapid spin interchange occurs at this temperature. New absorptions are observed in the centre of the spectra below 285 K. The spectra consist of an overlap of the absorptions of the low-spin isomer with those for the high-spin isomer.

Differential Scanning Calorimetry.—Figure 7 shows the d.s.c. curve for [Fe(py)L]BPh_4 for an increasing-temperature sequence, along with the temperature dependence of the magnetic moments. In the d.s.c. curve, a point of inflection at *ca.* 250 K toward the endothermic direction and an exothermic peak around 307 K were observed. The d.s.c. measurements for several discontinuous types of iron(III) spin-transition complexes have been carried out, and an endothermic peak for an increasing temperature sequence has been observed in the narrow temperature range in which the low-spin $\rightleftarrows$ high-spin spin transition is completed.[19,20] On the other hand, the temperature dependence of the magnetic moments for the present complex indicated that the spin transition took place over a wide range of temperature (150—330 K), and a broad endothermic change was observed between 249 and 300 K. Although the subsequent exothermic peak at 307 K probably due to a structural change should be related to the transition from low spin to high spin, the detail remains uncertain at present.

Crystal and Molecular Structure of [Fe(4Me-py)L]BPh_4.—The perspective drawings of [Fe(4Me-py)L]BPh_4 with the atom numbering schemes are shown in Figure 8. Listings of bond distances and bond angles are given in Tables 5 and 6, respectively. The iron atom assumes a pseudo-octahedral co-ordination with a *trans* geometry for the two salicylideneiminato-moieties, in which the basal plane comprises the N_2O_2 donors of these two moieties and the two axial positions are occupied by the secondary amine nitrogen atom of the di(3-aminopropyl)amine moiety and the nitrogen atom of 4-methylpyridine. The basal plane defined by Fe, O(1), O(2), N(1), and N(3) assumes a slight tetrahedral distortion, the deviations of the constituent atoms from the least-squares plane FeO_2N_2 being from −0.03 to 0.04 Å, and the dihedral angle between the planes Fe–O(1)–N(1) and Fe–O(2)–N(3) is 3.1°. Two salicylideneiminato-moieties construct a shallow 'cave' (or 'bow' shape), in which the 4Me-py ligand is positioned, where the depth of the cave can be estimated (by the atom deviations from the FeO_2N_2basal plane) to be 1.99 Å for C(5) and 1.61 Å for C(17). The dihedral angle between the two benzene rings of the two salicylideneiminato-moieties is 130.0°. The dihedral angle between the 4-methylpyridine plane and the FeO_2N_2 basal plane is 90.2°. The projection of the 4-methylpyridine plane onto the FeO_2N_2 basal plane makes an angle of 39.6° with the O(1)–Fe–N(4) plane, and the 4-methylpyridine plane bisects angle O(1)–Fe–N(3). The saturated six-membered chelate ring A has an envelope conformation, where the atoms C(8), C(9), and C(10) deviate by 1.09, 1.15, and 0.35 Å, respectively,

Table 7. Magnetic moments ($\mu_{eff.}$) and average metal–ligand distances (Å) for some iron(III) complexes with N_4O_2 donors[a]

Ref.	Complex	$\mu_{eff.}$	<Fe–N>	<Fe–O>	<Fe–Y>[b]
2	$[Fe(saldao)]Cl\cdot 2H_2O$	2.0	1.968	1.884	1.040(2)
5	$[Fe(saldad)]NO_3$	2.2	1.982(4)	1.878(4)	1.948(4)
2	$[Fe(saldao)]NO_3\cdot H_2O$	2.5	1.966	1.882	1.939(2)
2	$[Fe(taoddo)]PF_6$	5.9	2.136	1.930	2.068(3)
2	$[Fe(dctaoddo)]PF_6$	5.9	2.135	1.908	2.059(7)
5	$[Fe(saldaud)]NO_3$	6.0	2.152(3)	1.937(2)	2.080(3)
c	$[Fe(4Me\text{-}py)L]BPh_4$	3.5	2.006(6)	1.885(5)	1.965(6)

[a] Ligand abbreviations: saldad = 4,7-diazadecamethylene-1,10-bis(salicylideneiminate), saldaud = 4,8-diazaundecamethylene-1,11-bis(salicylideneiminate), saldao = 3,6-diazaoctamethylene-1,8-bis(salicylideneiminate), taoddo = 5,8,11,14-tetra-azaoctadeca-2,4,14,16-tetraene-2,17-diolate, dctaoddo = 3,16-dichloro-5,8,11,14-tetra-azaoctadeca-2,4,14,16-tetraene-2,17-diolate. [b] Y = N or O. [c] This work.

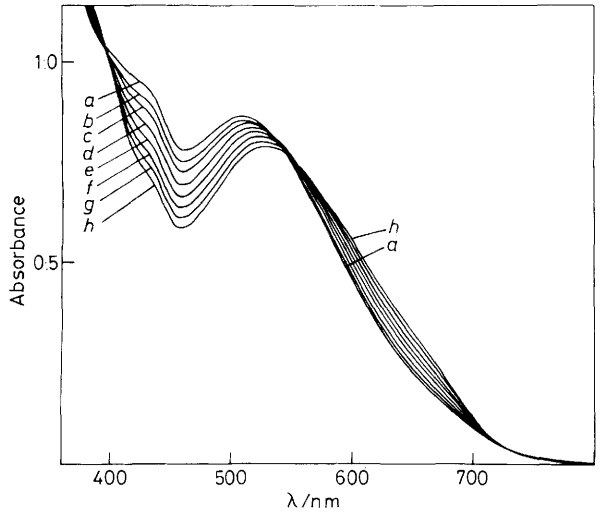

Figure 9. Temperature dependence of the electronic spectra for $[Fe(py)L]BPh_4$ (2.463×10^{-4} mol dm^{-3}) in dichloromethane solution: (*a*) 8.0, (*b*) 4.0, (*c*) 0.0, (*d*) −5.0, (*e*) −10.0, (*f*) −15.0, (*g*) −20.0, (*h*) −25.0 °C

from the plane defined by Fe, N(1), and N(2). The other six-membered chelate ring B has a chair conformation, where the atoms Fe and C(12) deviate by −1.00 and 0.44 Å, respectively, from the plane defined by N(2), N(3), C(11), and C(13). It should be noted that the thermal parameters for the carbon atoms of the saturated six membered chelate rings A and B are large compared with those of the other non-hydrogen atoms. It can be considered that a slight conformational change of the chelate rings reflects the tetrahedral distortion of the FeO_2N_2 basal plane and the iron–ligand bond lengths, and as a result it induces the spin transition, although this remains uncertain at present. Structural analyses of the high-temperature phase (high-spin isomer) and the low-temperature phase (low-spin isomer) are required.

It is known that the iron–ligand distances for iron(III) complexes with porphyrin derivatives, dialkyldithiocarbamates, or sexidentate Schiff-base ligands are affected by the spin state of iron(III).[2,5,21,22] The average iron–ligand distances and effective magnetic moment of the present complex as well as those of the high- and low-spin complexes with N_4O_2 donors are summarized in Table 7. The average iron–ligand distance in the high-spin complex is longer by *ca.* 0.12 Å than that in the low-spin complex.[2,5] The magnetic moment for the present complex is 3.45 B.M. at the temperature which the *X*-ray diffraction study was performed. By assuming a simple additive property for the magnetic susceptibility, where the limiting values for high- and low-spin states are taken as 2.00 and 5.90 B.M., the high-spin population (x) at this temperature (293 K) is estimated to be 0.26. The average iron–ligand distance for the present complex is close to that of the low-spin complex, rather than that of the high-spin complex, being consistent with the magnetic properties.

Spin Equilibrium in Solution.—The iron(III) complexes containing pyridine, imidazole, or their derivatives as an axial ligand showed thermochromic behaviour in various organic solvents, changing colour from dark violet to blue green on decreasing the temperature. Figure 9 shows the temperature dependence of the electronic spectra for $[Fe(py)L]BPh_4$ in dichloromethane solution. At 8.0 °C the spectrum exhibits two absorptions at 430 and 510 nm with absorption coefficients of 2 650 and 2 440 dm^3 mol^{-1} cm^{-1}, respectively. On decreasing the temperature, the absorption at 430 nm decreases in intensity and that at 510 nm shifts to higher wavelength with a decrease in intensity. The temperature dependence of the spectra should be due to the spin equilibrium between the high- and low-spin states. It can be considered that the high-spin species exhibits two absorptions at *ca.* 430 and 500 nm, and the low-spin species exhibits an absorption at *ca.* 530 nm, although a deconvolution analysis of the spectra is necessary.

Acknowledgements

We thank Professor Sigeo Kida at the Faculty of Science, Kyushu University, for use of the *X*-ray diffractometer. We also wish to thank the Institute for Molecular Science, Okazaki, and Professor Tasuku Ito for use of the electronic spectrophotometer. This work was partially supported by a grant-in-aid for scientific research from the Ministry of Education, Science and Culture.

References

1 Y. Tanabe and S. Sugano, *J. Phys. Soc. Jpn.*, 1954, **9**, 753.
2 E. Sinn, G. Sim, E. V. Dose, M. F. Tweedle, and L. J. Wilson, *J. Am. Chem. Soc.*, 1978, **100**, 3375.
3 M. F. Tweedle and L. J. Wilson, *J. Am. Chem. Soc.*, 1976, **98**, 4824.
4 R. A. Binstead, J. K. Beattie, T. G. Dewey, and D. H. Turner, *J. Am. Chem. Soc.*, 1980, **102**, 6642.
5 T. Ito, M. Sugimoto, H. Ito, K. Toriumi, H. Nakayama, W. Mori, and M. Sekizaki, *Chem. Lett.*, 1983, 121.
6 E. Frank and C. R. Abeledo, *Inorg. Chem.*, 1976, **5**, 1453.
7 L. Cambi and L. Szego, *Ber. Dtsch. Chem. Ges. B*, 1931, **64**, 2591.
8 M. Sugimoto, M. Nonoyama, T. Ito, and J. Fujita, *Inorg. Chem.*, 1983, **22**, 950.

9 M. Mikuriya, H. Okawa, and S. Kida, *Bull. Chem. Soc. Jpn.*, 1981, **54**, 2943.
10 H. Ohshio, Y. Maeda, and Y. Takashima, *Inorg. Chem.*, 1983, **22**, 2684.
11 T. Sakurai and K. Kobayashi, *Rikagaku Kenkyusho Hokoku*, 1979, **55**, 69; S. Kawano, *Rep. Comput. Cent. Univ. Kyushu*, 1980, **13**, 39.
12 'International Tables for *X*-Ray Crystallography,' Kynoch Press, Birmingham, 1974, vol. 4.
13 R. F. Stewart, E. R. Davidson, and W. T. Simpson, *J. Chem. Phys.*, 1965, **42**, 3175.
14 K. Nakamoto, 'Infrared and Raman Spectra of Inorganic and Coordination Compounds,' John Wiley & Sons, New York, 1978.
15 S. Koch, R. H. Holm, and R. B. Frankel, *J. Am. Chem. Soc.*, 1975, **97**, 6714.
16 E. König, G. Ritter, and S. K. Kulshreshtha, *Inorg. Chem.*, 1984, **23**, 1144.
17 E. König, G. Ritter, S. K. Kulshreshtha, J. Waigel, and L. Sacconi, *Inorg. Chem.*, 1984, **23**, 1241.
18 Y. Maeda and Y. Takashima, *Mem. Fac. Sci. Kyushu Univ., Ser. C*, 1983, **14**, 107.
19 M. Sorai and S. Seki, *J. Phys. Chem. Solids*, 1974, **35**, 555.
20 E. König, G. Ritter, S. K. Kulshreshtha, J. Waigel, and H. A. Goodwin, *Inorg. Chem.*, 1984, **23**, 1896.
21 D. K. Geiger, Y. J. Lee, and W. R. Scheidt, *J. Am. Chem. Soc.*, 1984, **106**, 6339.
22 J. G. Leipoldt and P. Coppens, *Inorg. Chem.*, 1973, **12**, 2269.

Received 15*th February* 1985; *Paper* 5/262